

# Breaking the Cycle: Short Recurrence and Overshoot of an M9-class Kamchatka Earthquake

Yuji Yagi 👓 \* 1, Yukitoshi Fukahata 👓 2, Ryo Okuwaki 🙃 1, Tomohiro Takagawa 🙃 3, Shinji Toda 🙃 4

<sup>1</sup>Institute of Life and Environmental Sciences, University of Tsukuba, Tennodai 1-1-1, Tsukuba, Ibaraki 305-8572, Japan, <sup>2</sup>Disaster Prevention Research Institute, Kyoto University, Gokasho, Uji, Kyoto, 611-0011, Japan, <sup>3</sup>Tsunami and Storm Surge Research Group, Port and Airport Research Institute, National Institute of Maritime, Port and Aviation Technology, 1-1-3, Nagase, Yokosuka, 239-0826, Japan, <sup>4</sup>International Research Institute of Disaster Science (IRIDeS), Tohoku University, 468-1 Aoba, Aramaki, Aoba-ku, Sendai, 980-8572, Japan

#### **Text S1: Methods**

### **Back projection**

The back-projection (BP) method (Ishii et al., 2005; Krüger and Ohrnberger, 2005) is a technique to infer the spatiotemporal distribution of the seismic source by stacking observed waveforms after time-shifting them with theoretical travel times. In the BP analysis, we used the same observation stations as in the PDTI analysis, and the 20 Hz sampled waveforms were band-pass filtered between 0.05 and 0.15 Hz. In general, the BP method is insensitive to variations in depth, and therefore the model-plane geometry was not calibrated. The model plane was set up following the PDTI analysis, with a strike angle of 218°, dip angle of 16° and a hypocentral depth of 30 km. The knot spacing was set to 10 km in both the strike and dip directions. The travel time was computed using TauP (Crotwell et al., 1999) with the AK135 velocity model (Kennett et al., 1995; Montagner and Kennett, 1996).

# **Processing of tsunami waveforms**

For the 1952 event, tsunami waveforms from all stations except Hakodate were downloaded from the National Oceanic and Atmospheric Administration (NOAA) Center for Tsunami Research (NOAA National Centers for Environmental Information; NOAA Center for Tsunami Research, 2017). The analog record from the Hakodate station, published in a report by Inouye (1953), was digitized. Tsunami waveforms for the 2025 event were downloaded from the Sea Level Station Monitoring Facility (Flanders Marine Institute (VLIZ); Intergovernmental Oceanographic Commission (IOC), 2021). For both the 1952 and 2025 events, a zero-phase high-pass filter with a corner period of three hours was applied to the tsunami waveforms to remove tidal effects.

### Tsunami simulation

Vertical displacements of the initial water level due to seafloor deformation are calculated from the fault parameters assuming a semi-infinite elastic medium based on the formulation by Okada (1992). The fault parameters are from our PDTI solution (Fig. 1d), which is re-mapped into 10 km x 10 km rectangular subfaults, where the corresponding potency is given. The input PDTI solution was based on a model plane with a dip angle of 16° and the modified regional structure model of the Kamchatka Peninsula (Fig. 1d). The distribution of the initial water level is given by the seafloor displacements without considering dynamic rupture effects (Fig. S7b). The simulated waveforms are computed using the adjoint synthesis method by Takagawa et al. (2024) (Fig. S7c), which considers the effects on the seawater compressibility, seafloor deformation due to tsunami loading, gravitational potential change, and Boussinesq dispersion. The bathymetry data were generated by down-sampling the GEBCO\_2023 Grid (GEBCO Compilation Group, 2023) to 30 arc-second intervals.

<sup>\*</sup>Corresponding author: yagi-y@geol.tsukuba.ac.jp

**Table S1** Near-source underground structure from CRUST 1.0 (Laske et al., 2013).

$V_P$ (km/s)	$V_S$ (km/s)	Density (10 <sup>3</sup> kg/m <sup>3</sup> )	Thickness (km)
1.500	0.000	1.020	3.590
5.000	2.700	2.550	4.180
6.500	3.700	2.850	3.250
7.100	4.050	3.050	10.050
8.010	4.450	3.300	- (Moho)

**Table S2** Near-source underground structure from Nizkous et al. (2007).

$V_P$ (km/s)	$V_S$ (km/s)	Density (10 <sup>3</sup> kg/m <sup>3</sup> )	Thickness (km)
1.450	0.000	1.020	4.000
5.800	3.460	2.500	6.000
6.850	3.860	2.700	20.000
7.450	4.300	3.100	10.000
7.700	4.500	3.200	- (Moho)

**Table S3** Near-source underground structure from AK135 (Kennett et al., 1995; Montagner and Kennett, 1996).

$V_P$ (km/s)	$V_S$ (km/s)	Density (10 <sup>3</sup> kg/m <sup>3</sup> )	Thickness (km)
1.450	0.000	1.020	4.000
5.800	3.460	2.449	16.000
6.500	3.850	2.714	15.000
8.040	4.480	3.298	- (Moho)

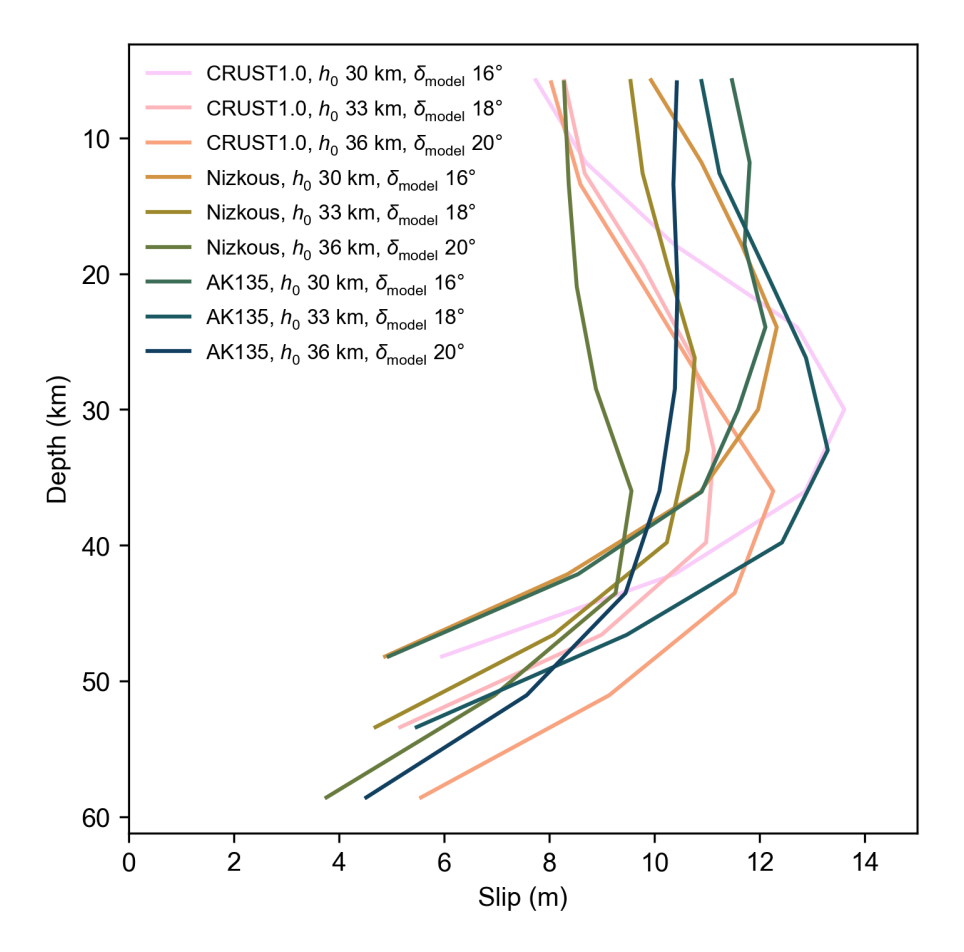


**Figure S1** Compilation of PDTI models in depth. Each line represents the maximum slip amount at each along-dip grid location.

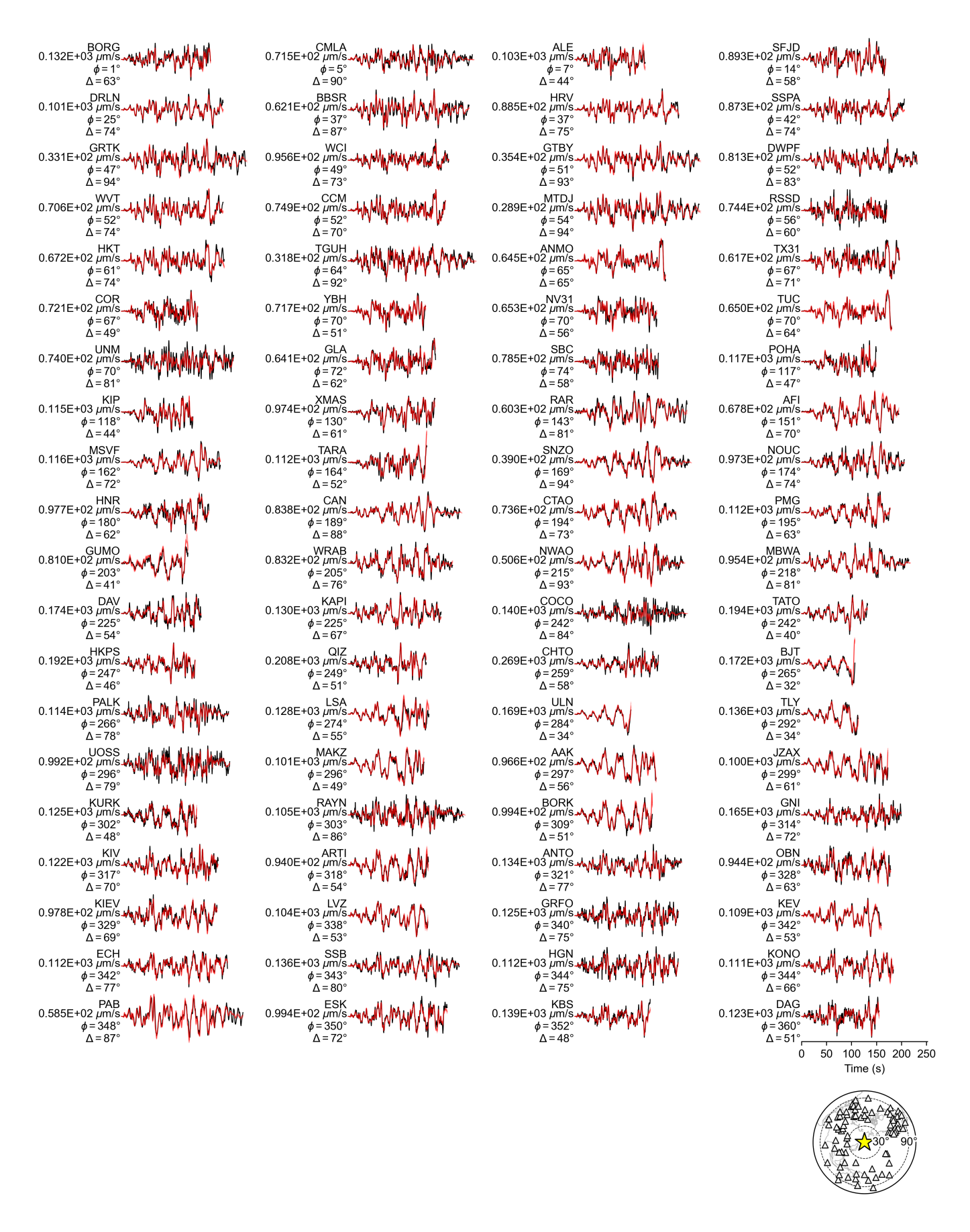


**Figure S2** Observed and synthetic waveforms of all models. Observed waveforms (black) were converted to velocity at a 20 Hz sampling rate, with an anti-aliasing filter applied. Synthetic waveforms for each model are shown in semi-transparent red. Also shown are the station code, the maximum amplitude of the observed waveforms, the azimuth and the epicentral distance for each station. The station locations are plotted on the inset map at lower right corner.

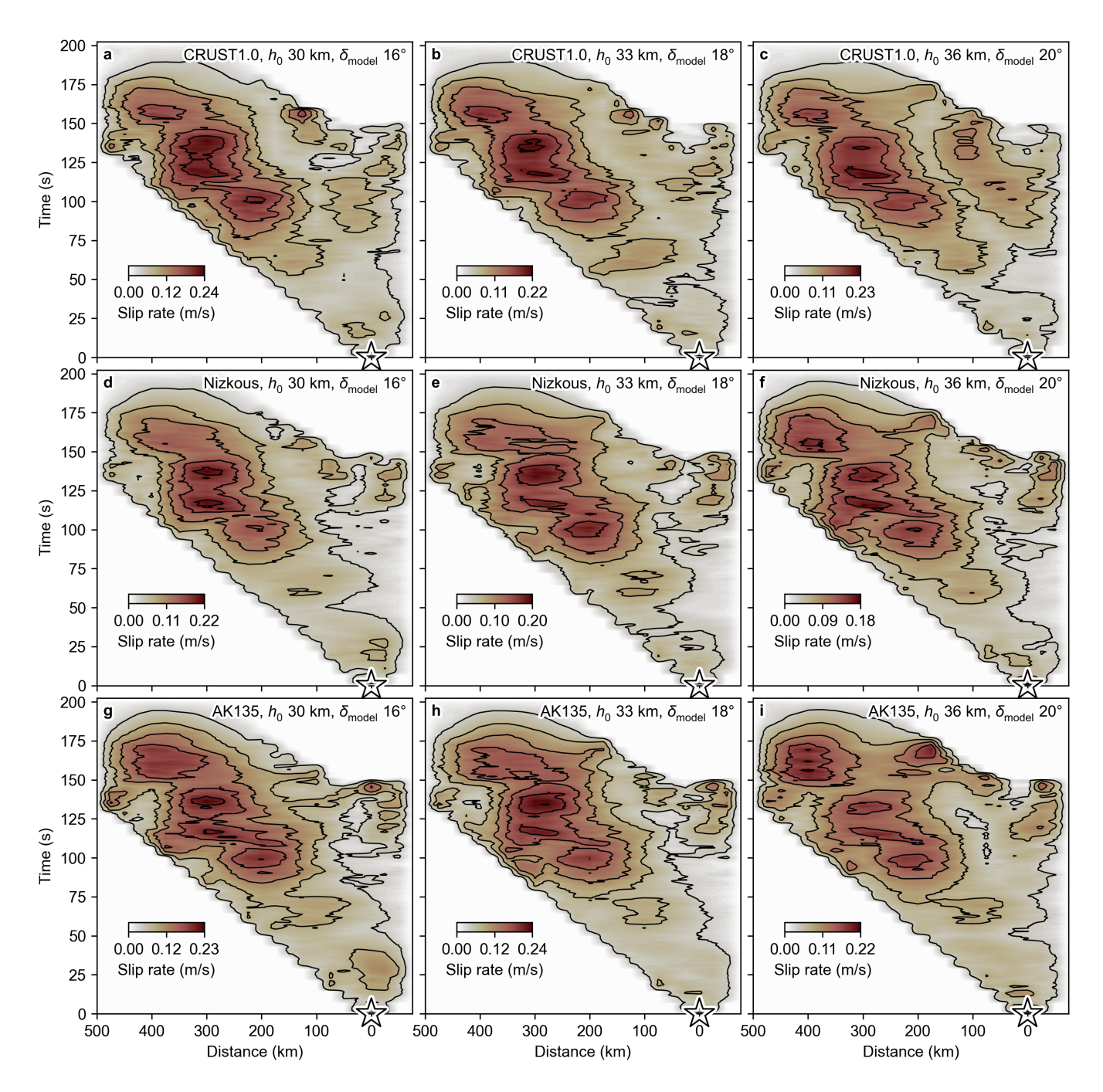


**Figure S3** Rupture growth of the 2025 Kamchatka earthquake for all models. (a–i) Spatiotemporal distributions of slip rate, projected along strike, for all models. The horizontal axis denotes the along-strike distance from the hypocentre. The upper-right label in each panel indicates the model configuration (near-source understructure model, initial rupture depth and fault-plane dip angle). The maximum slip rate matches the upper limit of the colour scale, and contour intervals are set to one fifth of the maximum value.

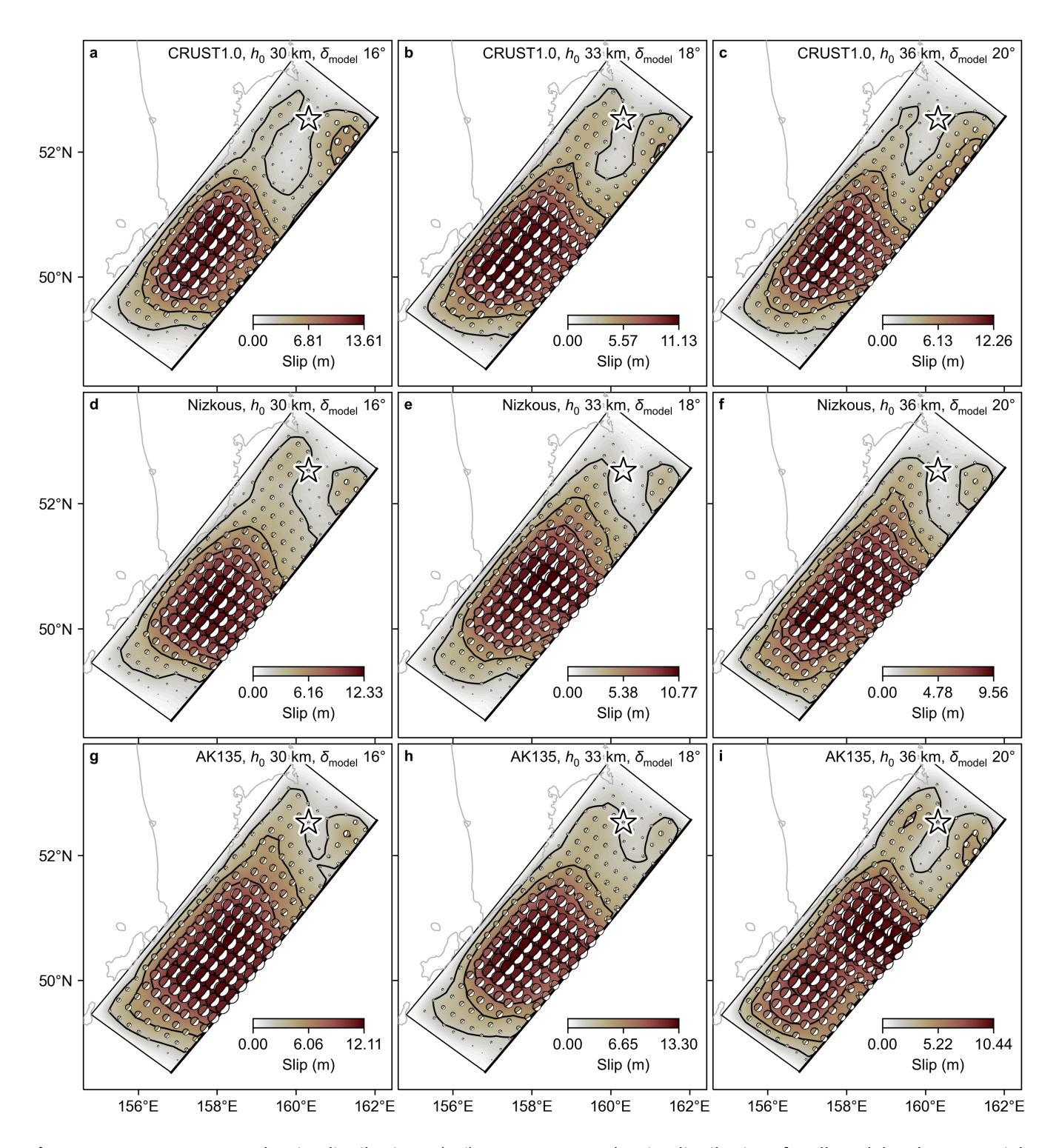


**Figure S4** Potency tensor density distributions. (a–i) Potency tensor density distributions for all models. The upper-right label in each panel indicates the model configuration (near-source understructure model, initial rupture depth and model-plane dip angle). The maximum potency density (corresponding to slip) for each model matches the upper limit of the colour scale, and contour intervals are set to one fifth of the maximum value. The moment tensor solution from the potency density tensor is projected onto the map using the lower hemisphere projection.

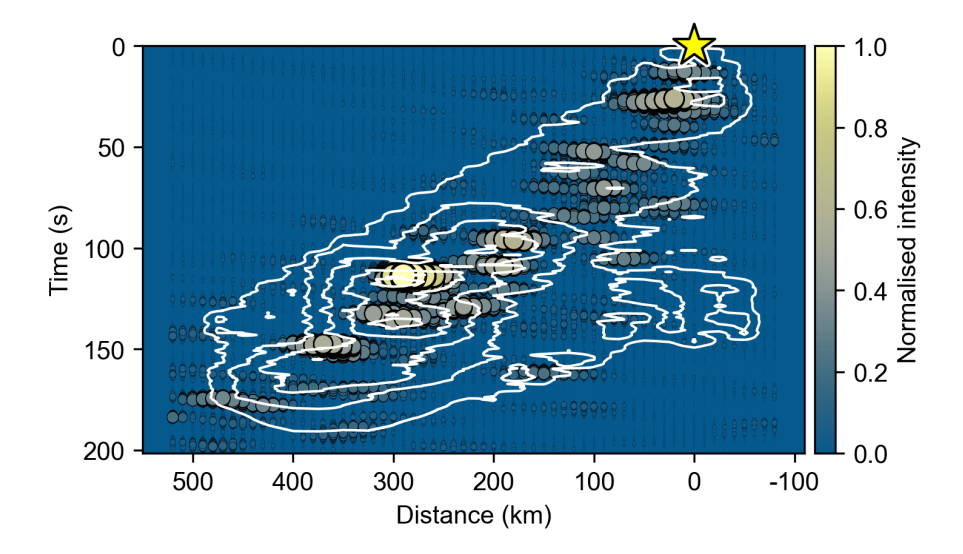


**Figure S5** Comparison of BP image and PDTI solution. The white contours show the temporal evolution of slip rate projected along the fault-plane strike, which is the same as shown in Fig. 2b. Contour intervals are 0.04 m/s. The scatter plots indicate the normalized intensity of the BP image, and marker size is scaled according to the normalized intensity.

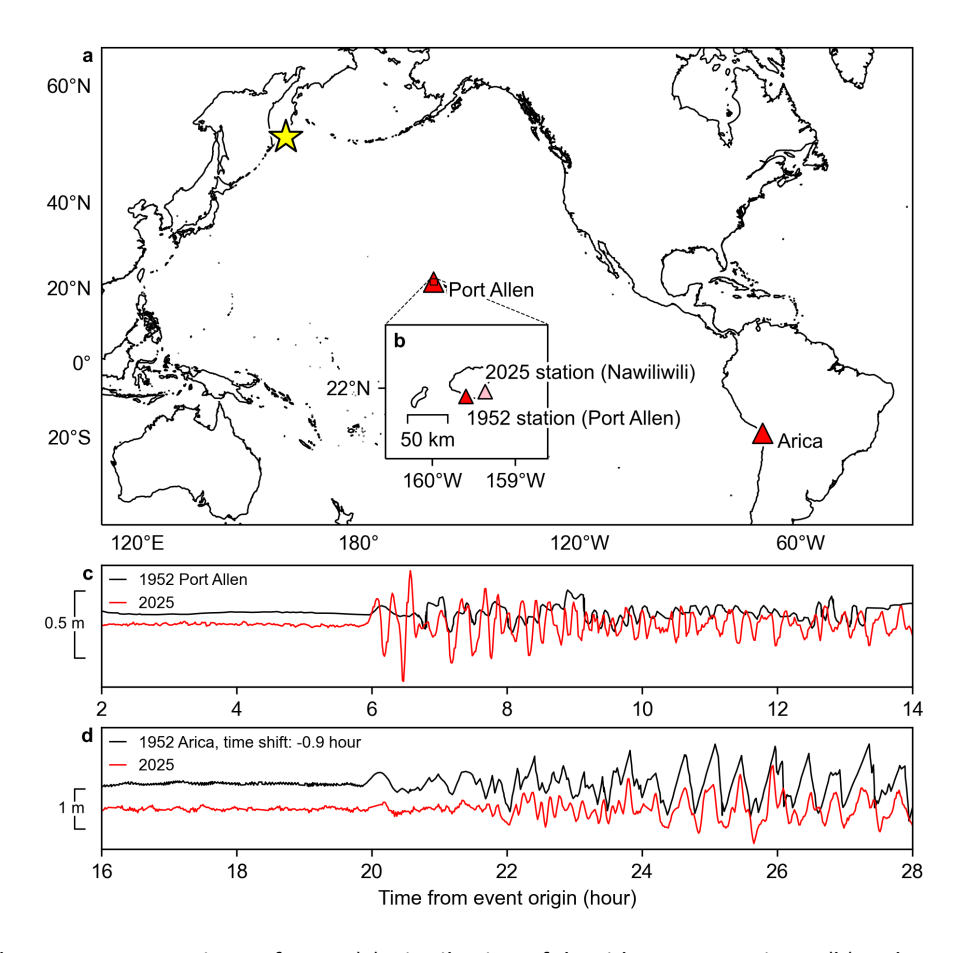


**Figure S6** Supplementary tsunami waveforms. (a) Distribution of the tide-gauge stations. (b) A close-up view of the tide-gauge stations for the 1952 and 2025 records shown in (c). (c,d) Tsunami waveforms recorded at coastal tide gauges for the 1952 (black) and 2025 (red) events. A zero-phase high-pass filter with a corner period of 3 hour was applied to remove tidal effects. The 1952 record at the Arica station is time-shifted by -0.9 hours.

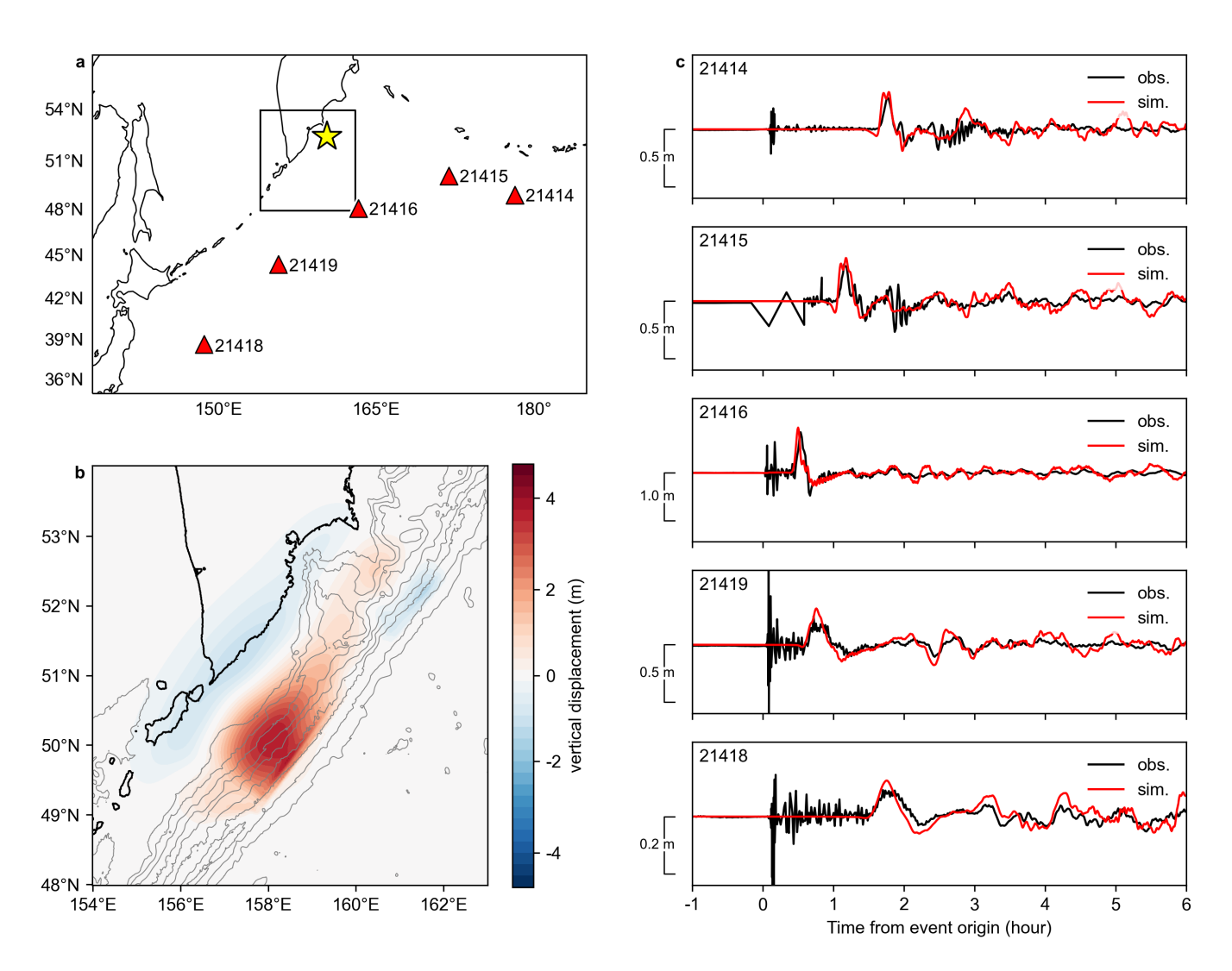


**Figure S7** Tsunami simulation for the 2025 event. (a) The star indicates the 2025 epicentre. The triangles are the DART buoy stations along with the station codes. The rectangle shows the area of the panel (b). (b) The colour contour shows the vertical displacement of the seafloor for the initial water level calculated from the PDTI solution. The grey contours show the bathymetry. (c) The comparison between the observed (black) and the simulated (red) waveforms.

# References

- Crotwell, H. P., Owens, T. J., and Ritsema, J. The TauP Toolkit: Flexible Seismic Travel-time and Ray-path Utilities. *Seismol. Res. Lett.*, 70(2): 154–160, mar 1999. doi: 10.1785/gssrl.70.2.154.
- Flanders Marine Institute (VLIZ); Intergovernmental Oceanographic Commission (IOC). Sea level station monitoring facility, 2021. doi: 10.14284/482.
- GEBCO Compilation Group. GEBCO 2023 Grid, 2023. doi: 10.5285/f98b053b-0cbc-6c23-e053-6c86abc0af7b.
- Inouye, W. Report on the investigation of the Kamchatka earthquake of November 1952 (in Japanese). *Q. J. Seismol.*, 18:5–48, 1953. https://www.jma.go.jp/jma/kishou/books/kenshin/vol18p005.pdf.
- Ishii, M., Shearer, P. M., Houston, H., and Vidale, J. E. Extent, duration and speed of the 2004 Sumatra-Andaman earthquake imaged by the Hi-Net array. *Nature*, 435(7044):933–936, 2005. doi: 10.1038/nature03675.
- Kennett, B. L., Engdahl, E. R., and Buland, R. Constraints on seismic velocities in the Earth from traveltimes. *Geophys. J. Int.*, 122(1):108–124, 1995. doi: 10.1111/j.1365-246X.1995.tb03540.x.
- Krüger, F. and Ohrnberger, M. Tracking the rupture of the Mw = 9.3 Sumatra earthquake over 1,150km at teleseismic distance. *Nature*, 435 (7044):937–939, 2005. doi: 10.1038/nature03696.
- Laske, G., Masters, T. G., Ma, Z., and Pasyanos, M. Update on CRUST1.0 A 1-degree Global Model of Earth's Crust. https://igppweb.ucsd.edu/~gabi/crust1.html, Geophys. Res. Abstr. 15, Abstr. EGU2013-2658, 15:Abstract EGU2013-2658, 2013.
- Montagner, J.-P. and Kennett, B. L. N. How to reconcile body-wave and normal-mode reference earth models. *Geophys. J. Int.*, 125(1): 229–248, apr 1996. doi: 10.1111/j.1365-246X.1996.tb06548.x.
- Nizkous, I., Kissling, E., Sanina, I., Gontovaya, L., and Levina, V. Correlation of Kamchatka lithosphere velocity anomalies with subduction processes. In *Geophys. Monogr. Ser.*, volume 172, pages 97–106. 2007. doi: 10.1029/172GM09.
- NOAA National Centers for Environmental Information; NOAA Center for Tsunami Research. Archival and Discovery of November 4, 1952 Tsunami Event on Marigrams, 2017. doi: 10.7289/V55H7DGQ.
- Okada, Y. Internal deformation due to shear and tensile faults in a half-space. *Bull. Seismol. Soc. Am.*, 82(2):1018–1040, apr 1992. doi: 10.1785/BSSA0820021018.
- Takagawa, T., Allgeyer, S., and Cummins, P. Adjoint Synthesis for Trans-Oceanic Tsunami Waveforms and Simultaneous Inversion of Fault Geometry and Slip Distribution. *J. Geophys. Res. Solid Earth*, 129(6):e2024JB028750, jun 2024. doi: 10.1029/2024JB028750.